CLM-P184

This document is intended for publication in a journal, and is made available on the understanding that extracts or references will not be published prior to publication of the original, without the consent of the authors.

CULHAM LIBRARY
REFERENCE ONLY

21SEP1990

United Kingdom Atomic Energy Authority
RESEARCH GROUP

Preprint

THE STABILITY OF A BULGED REGION IN THE MIDPLANE OF A LONG THETA PINCH

H. A. B. BODIN
A. A. NEWTON
G. H. WOLF
J. A. WESSON

Culham Laboratory
Abingdon Berkshire

1969

Enquiries about copyright and reproduction should be addressed to the
Librarian, UKAEA, Culham Laboratory, Abingdon, Berkshire, England

UNCLASSIFIED
(Approved for Publication)

CLM-P 184

THE STABILITY OF A BULGED REGION IN THE MIDPLANE OF A LONG THETA PINCH

by

H.A.B. Bodin
A.A. Newton
G.H. Wolf*
J.A. Wesson

*Permanent address Institut für Plasmaphysik,
Garching bei Munchen, Germany

U.K.A.E.A. Research Group,
Culham Laboratory,
Abingdon,
Berks.

July, 1969

A B S T R A C T

An experimental and theoretical study has been made of the hydromagnetic instability of an axisymmetric bulged region in the midplane of a theta pinch 8 metres long. The bulged region was generated adiabatically after the initial implosion in such a way that it fulfilled most of the assumptions of the theoretical model; in particular, it was free of end effects for the time of observation. At a filling pressure of 20 mtorr D_2 and with a peak magnetic field of 20 kG the plasma, which was collision dominated, had values of temperature, density and beta on the axis of 120 eV, 3×10^{16} cm^{-3} and 0.7 ± 0.2. The predicted $m = 1$ instability was observed and for a range of bulge amplitudes its measured growth and propagation along the column agreed to within a factor of less than two with the theoretical values. It is concluded that the $m = 1$ instability of such bulged plasmas is well described by ideal MHD theory. Modes with $m \geqslant 2$ were not observed during the $m = 1$ growth and their absence is attributed to finite Larmor radius stabilisation.

CONTENTS

I. INTRODUCTION

Several years' study of the theta pinch has shown that deuteron temperatures of up to a few keV can be achieved at densities in the range $10^{16} - 10^{17}$ cm^{-3}[1-5]. Most work has concerned the mechanisms of heating[2,3], energy loss[6] and particle losses[2,4,5,7]. Observations have also been made of the naturally occurring instabilities[2,4,8-12] which fall into three categories. The first is the Rayleigh-Taylor instability, commonly observed during the implosion phase in low temperature theta pinches[8,9]; it is damped in higher temperature discharges[10]. The second is the $m = 2$ rotational instability[13], and the third is the resistive tearing mode observed in the reversed field configuration[11].

Also instabilities in regions of adverse magnetic field line curvature have been studied in short coils with magnetic mirrors[14-16], in a long corrugated coil[17], in reversed field theta-pinches with closed field lines[18-20] and in the toroidal M & S Theta Pinch[21,22]. Short wavelength (high m-number) instabilities, expected to have high growth rates for thin current sheaths, were rarely observed in these experiments. At low filling pressures[1-5] their absence may be due to finite Larmor radius effects[23-25]; in addition, diffuse current sheaths were usually observed for which ideal MHD theory predicts the growth rates of all m-modes[26,27,29] to be approximately equal to that for $m = 1$ with a thin sheath[28]. Thus, although the length of the pinches studied had been progressively increased to two metres the MHD growth times for all modes become comparable to the transit time of a hydromagnetic wave along the system, so that end effects such as plasma or heat flow, line tying or the favourable curvature of field lines outside the coil can no longer be neglected. These

end effects are expected either to reduce the MHD growth rate or to give stability.

Theoretical work based on the ideal MHD model[27-32] has been carried out; when β is sufficiently high a theta-pinch of finite length can be stable[29] due to the regions with favourable curvature at the ends. In infinite columns with either periodic bulges or a single bulged region and $\beta < 1$, the plasma is predicted to be unstable to all modes $m \geqslant 1$, for both sharp and diffuse radial pressure distributions in the absence of conducting walls. All modes can be stabilised by conducting walls[29], but only for values of β near unity, and for low compression ratios.

In the experiment described here an MHD unstable axisymmetric bulged configuration was generated adiabatically in the midplane of the coil and the growth of the observed $m = 1$ instability was compared with calculations based on ideal MHD theory. This configuration (which is the linear analogue of one bulge of the toroidal M & S system[33-35]), was chosen because it is amenable to theoretical analysis and it can be set up experimentally in such a way that the assumptions of the theory are adequately satisfied. With the 8 metre long coil the plasma was uninfluenced by the ends for many instability growth times and its length was thus effectively infinite for the time scale of the experiment. The growth rates of the observed $m = 1$ instabilities agreed with the predictions of ideal MHD theory. Higher modes did not grow and are believed to be damped by non-ideal effects. Measurements of the plasma temperature and density[36] and its radial diffusion[37a] are reported elsewhere[37b].

II. THEORY

This Section deals with the theory of an $m = 1$ instability in

a long initially axisymmetric plasma cylinder with a single bulged region. The initial equilibrium configuration is shown in Fig.1. The bulge is characterised by δ, the bulge strength, given by $(r_2 - r_1)/2r_1$ (where r_2 is the plasma radius in the midplane of the bulge and r_1 the radius in the uniform column) and its length, L.

When the plasma is displaced a small amount ξ from the equilibrium position the variation in potential energy of the system is negative, showing instability. The variation comprises three terms; the surface magnetic energy, which drives the instability, volume magnetic energy, which is stabilising but small, and plasma energy. For the latter it has been shown[28] that the most unstable displacements do not change the plasma volume and therefore not its energy.

A normal mode analysis is used to describe the growth of the instability. Each axial mode is expressed in the form

$$\xi_n(z, t) = \hat{\xi}_n (z)\, e^{\omega_n t} \qquad \ldots (1)$$

where $\hat{\xi}_n$ is the initial amplitude of the mode n. For the values of δ and β in the present experiment one unstable axial mode dominates in the vicinity of the bulge. The growth rate calculated analytically for small δ (see Appendix I) is

$$\omega_{m=1} = 2\pi^2 \left(\frac{2}{\gamma} \right)^{\frac{1}{2}} \frac{\delta^2 C_S}{L} \frac{\beta_o^{\frac{1}{2}}(1-\beta_o)(3-2\beta_o)}{(2-\beta_o)^{\frac{3}{2}}} \qquad \ldots (2)$$

where the sound speed $C_S = \sqrt{\gamma k (T_e + T_i)/m_i}$ (γ is the ratio of specific heats and T_e, T_i are the electron and ion temperatures and m_i is the ion mass), and β_o is the ratio of plasma pressure to the confining magnetic pressure in the region of the uniform column. A square pressure profile is used in the theory and in order to compare it with experiment an average beta must be assumed (see Appendix II).

The growth rate has been computed for finite δ (see Appendix I and Figs.10 and 11).

The calculation takes into account contributions from the regions of favourable and unfavourable curvature and the mass loading due to plasma extending axially outside the bulged region. For given values of δ, L and β_o it follows from Eq.(AI.5) that differently shaped bulges have the same growth rates if they also have the same values of

$$\int_{-L/2}^{+L/2} (dr_p/dz)^2 \, dz$$

where r_p is the plasma radius. This shows that, in the absence of conducting walls, all axially symmetric bulged high-β configurations containing both stable and unstable curvature, and bounded by infinite uniform regions, are unstable. Because of the coupling between neighbouring regions of the column $\omega_{m=1}$ is always smaller than the growth rate calculated using only the contribution of unfavourable curvature. In the limit of small δ the growth for the latter case scales as $\delta^{\frac{1}{2}}$ compared with δ for a periodic bulged configuration and δ^2 for the single bulge considered in this paper. For large bulges the growth rates for the periodic and single bulged configurations are approximately the same (see also Fig.10 and Appendix I).

The growth of the instability is accompanied by a propagation of its amplitude along the column in the directions away from the bulge. This is seen in Eq.(AI.2) which, for the uniform column, leads to a simple wave equation with a velocity given, for finite β_o, by

$$V_{m=1} = V_A \sqrt{2 - \beta_o} = C_s \sqrt{2(2 - \beta_o)/\gamma\beta_o} \qquad \ldots (3)$$

where V_A is Alfven speed, defined using the density on the axis and the external magnetic field. Note that $V_{m=1}$ is always larger than

the ion thermal speed, usually by more than a factor of two. Thus it is not expected that in a collisionless plasma the ion thermal motion will increase coupling between different parts of the column and reduce the growth rate.

In addition $V_{m=1} > V_{m=0}$, the speed of the $m = 0$ rarefaction wave moving away from the bulge due to its formation ($V_{m=0} = V_A\sqrt{1-\beta_o}$); therefore any redistribution of mass due to plasma flow will not significantly affect the inertia of the plasma column in the vicinity of the unstable region.

The $m = 1$ propagation velocity can be used to estimate the minimum length of coil, Λ_{min}, required to ensure that end effects will not influence the growth of the instability at the coil midplane. To observe α growth times, $\alpha/\omega_{m=1} \geqslant \Lambda_{min}/2V_{m=1}$, from which

$$\frac{L}{\Lambda_{min}} \geqslant \frac{\pi^2}{\alpha}\frac{\delta^2}{} \frac{\beta_o(1-\beta_o)(3-2\beta_o)}{(2-\beta_o)^2} \qquad \ldots (4)$$

In a long coil the most important stabilising mechanism for $m = 1$ is the effect of conducting walls, which has been analysed for the periodic bulged configuration assuming small δ[29]. When the walls are close to the plasma the variation of the vacuum field energy (see above) dominates the destablising surface energy and stabilises if

$$\beta_o > \beta_{crit} = 1 - (r_p/r_w)^2 \qquad \ldots (5)$$

(r_w is the radius of the conducting wall). For the values of β_o and r_p/r_w in this experiment with a single bulge, the walls are unlikely to reduce the growth rate except at very large values of δ where beta tends to unity in the midplane of the bulge. Such wall effects have been neglected in deriving the theoretical growth rates.

Finite Larmor radius stabilisation, shown to apply for the values of beta appropriate to the present experiment[25], will not affect

$m = 1$ when there is no deformation of the column. However, it is expected to stabilise $m \geqslant 2$[23], i.e. modes which deform the plasma cross section, when

$$(a_i/r_2)^2 > \frac{\omega_m}{\Omega_i} \qquad \ldots (6)$$

where a_i is the ion Larmor radius, ω_m the ideal MHD growth rate and Ω_i the ion gyro-frequency. Damping of modes $m \geqslant 2$ due to a "collisionless viscosity" when the ion mean free path is much greater than the plasma radius and beta is almost unity over most of the plasma[38] is neglected in this work since these conditions do not occur.

III. EXPERIMENTAL DETAILS

A. Parameters of Experiment and Plasma Properties

The 8 metre experiment was operated in conditions already described[36,37]. For the instability studies a bank voltage of 34 kV was used at a deuterium filling pressure of 20 mtorr, which gives a peak electron density on the axis of about 3×10^{16} cm^{-3} and ion and electron temperatures of about 120 eV. The peak magnetic field of 20 kG was reached in 5·5 μsec and it decayed in 160 μsec. The value of beta on the axis is about 0·7. The plasma is collision-dominated, with a mean free path comparable with its diameter, and the Larmor radius of the ions is about 1 mm. The plasma is therefore expected to be well described by the MHD model.

The principal parameters of the experiment and some of the measured plasma properties are summarised in Table I. Thomson scattering was used to measure both the electron temperature and density; in addition, the latter was determined independently from the visible continuum emission[36,37].

In the absence of an unstable bulge the plasma remains close to the coil axis along its whole length for 25-30 μsec; thereafter an instability, which is a combination of $m = 1$ and $m = 2$, associated with a rotation of the column, is observed to grow simultaneously along the length. The measurements discussed in this paper were all obtained before the onset of this 'residual instability'. During this time there is a small amplitude (much less than the plasma radius) lateral motion of the plasma, which was due to small differences in the current and geometric arrangement of the independent coil sections; however, this low amplitude motion was not found to have any effect on the plasma behaviour.

B. Generation and Growth of the Unstable Bulge

In order to preserve the cylindrical symmetry of the plasma at early times the unstable bulge was generated after the initial implosion. The coil is divided into 32 separate sections each 24 cm long, with its own crowbar switch. One section, known as the field shaping coil, is short-circuited, an interval $\Delta t = t_1 - t_2$ (see Fig.2) before peak magnetic field and the field, B_2, within it rises more slowly than the field, B_1, elsewhere; plasma flows into this region and a bulge develops. The method is illustrated in Fig.2, where oscillograms of the magnetic fields are shown; there the discontinuity in B_2 at 2·5 μsec shows the start of field shaping. A minimum field ratio $B_2/B_1 = 0{\cdot}5$ can be produced with $\Delta t = 4$ μsec and the ratio can be continuously varied by changing Δt.

The structure of the vacuum field was studied using a low voltage analogue[42]. An axial gap of 0·5 cm between coils allowed the required field ratio to be obtained with the crowbar circuit oscillations in phase in adjacent coils. Distortions of the magnetic field

due to the collector feed slot gave rise to a small non-symmetrical radial component ($\sim 1\%\, B_2$) in the bulged field towards the feed slot, which was not expected to cause a measurable lack of lateral equilibrium[39,40] during the formation of the bulge and the growth of the instability (see also Sec.VI).

The bulge amplitude was determined at its midplane as a function of time from streak camera photographs which gave the average radii ($\langle r_p \rangle$ in Appendix II). Values of δ are plotted as a function of time in Fig.3 for various field shaping ratios, B_2/B_1. It can be seen that δ increases with time and the bulge reaches equilibrium only when $B_2/B_1 > 0{\cdot}75$. With smaller values of B_2/B_1 equilibrium is not reached[41].

For the case of a square pressure profile it can be shown from pressure balance and internal magnetic flux conservation that radial equilibrium is reached when

$$\frac{r_2}{r_1} = \left[\left(\frac{B_1}{B_2} \right)^2 \frac{1 - \beta_o}{1 - \beta_o \left(\frac{B_1}{B_2} \right)^2} \right]^{1/4} \qquad \ldots (7)$$

Note that Eq.(7) predicts no simple equilibrium for $(B_2/B_1)^2 < \beta_o$. For the measured equilibrium values of δ Eq.(7) is satisfied by $\beta_o = 0{\cdot}3$ to $0{\cdot}4$. The experimentally measured $\beta(r)$ is of Gaussian form[36,37] with a β_o on the axis of $0{\cdot}7 \pm 0{\cdot}2$ and the corresponding average value of β_o (i.e., $\langle \beta \rangle$ defined in Appendix II) of $0{\cdot}4 \mp 0{\cdot}1$ is in satisfactory agreement with the above observation.

IV. EXPERIMENTAL RESULTS ON THE INSTABILITY

Fig.4 shows a series of stereoscopic framing and streak camera photographs taken in the neighbourhood of the unstable bulge. The arrow (S) on the framing photograph shows the position viewed by the streak camera; the arrow (F) on the streak photograph indicates the time when the framing photograph was taken. (A) and (B) correspond to cameras viewing the plasma 45^{o} above and below the plane of the collector feed slot (see also Fig.5). The four pairs of photographs in Fig.4 correspond to different field ratios B_2/B_1 from 1 to 0.64. The framing photographs are on the left hand side of the figure and show the shaped region and the neighbouring section of the column. These were taken 6 μsec after the start of the discharge with 1 μsec exposure time. The extent of the bulged region can be clearly seen. For strong bulges there is a marked reduction in the intensity of the light coming from the very end of the shaped region and this is due to an $m = 0$ rarefaction wave moving outwards from the shaped regions along the column, as plasma flows in to fill the bulge[41].

Corresponding streak photographs (right hand side of Fig.4) taken through the gap between the shaped and unshaped coils show the $m = 1$ instability. The growth rate increases and the time at which the plasma strikes the walls decreases as B_2/B_1 is reduced. The low amplitude lateral motion present with no field shaping is seen in the top photograph. Modes with $m \geqslant 2$ did not appear in the available observation time before the plasma hit the walls due to the $m = 1$ instability.

Fig.5 shows the motion of the plasma axis during the growth of the instability. The instability drives the plasma in a plane inclined at about 45^{o} from the plane of the collector plate feed point.

Although there is some variation in the motion of the plasma from one discharge to another, the tendency to move in the same general direction, even for $B_2/B_1 = 1$, indicates that some initial disturbance of the plasma from its equilibrium position determines the direction in which it will move. This may also explain the observation that during the formation of the bulge a rapid displacement of up to 4 mm occurred which was independent of B_2/B_1. This was followed by an exponentially growing displacement to the wall for $B_2/B_1 < 0{\cdot}75$. For $B_2/B_1 > 0{\cdot}75$ however, the plasma did not reach the wall and its motion was damped or even reversed at large displacements.

The displacement, ξ, of the plasma axis from its initial average position is plotted as a function of time in Fig.6. The values of $\xi(t)$ were not corrected for the residual motion observed with no field shaping. A well defined exponential growth of $\xi(t)$ can be seen which becomes faster as B_2/B_1 decreases. (The apparent difference in time scales between the growth of the bulge (Fig.3) and that of the instability is because they were measured at different axial positions (see Fig.4)).

Because the bulges continue to grow while the instability develops an average value of δ must be used. The theory is likely to be most accurate for small δ so we take the effective value, δ_{eff}, to be that reached after 1·3 growth times of the instability, chosen since after that time equilibrium is reached for the weak bulges. This is shown in Fig.3, where points corresponding to 1·3 growth times are marked. These fall on a straight line because for the values of δ studied $\omega_{m=1} \propto \delta$.

Growth rates are plotted against the effective δ in Fig.7, where each point represents one discharge. The errors shown on δ_{eff} come from the measurements of r_1 and r_2 and do not include the uncertainty in its definition (see above). Also shown are growth rates calculated from theory assuming $C_s = 1{\cdot}4 \times 10^7$ cm sec^{-1}, $\langle\beta\rangle = 0{\cdot}38$, and $L = 25$ cm.

V. EXPERIMENTAL RESULTS ON THE m = 1 WAVE

Fig.8 shows a streak photograph of the $m = 1$ motion of the plasma column for three different values of the axial distance, z, measured from the midplane of the unstable bulge. These streak pictures are used to evaluate the onset time of the $m = 1$ motion as a function of z, as plotted in Fig.9. The onset time for $z = 0$ was deduced from Fig.4.

VI. DISCUSSION

The data presented in Figs.6 and 7 showed that an exponentially growing $m = 1$ instability can be induced by forming a bulge. The growth rate agrees with ideal MHD theory for small bulges, but appears to become independent of δ for large bulges. The $m = 1$ wave due to the instability was found to propagate along the column at the predicted velocity (Fig.9). In order to assess the validity of this comparison we now discuss some of the assumptions which were made.

Firstly there is the assumption that theory for an infinite column may be used, i.e. that the ends do not influence the instability. End effects can occur in four ways: (i) propagation of the $m = 1$ wave outwards to couple to the favourable curvature outside the coil; this takes more than 20 μsec (see Fig.9); (ii) propagation of hydromagnetic waves in from the end takes 20–30 μsec, as evidenced

by the onset of the residual instability in the theoretically expected time; (iii) axial loss of particles from the midplane at thermal speeds; the line density was observed to be constant for at least 25 μsec and theoretically should remain so for $t = \Lambda/2C_s \approx 35$ sec[4,7,43] and (iv) loss of heat by thermal conduction[6], expected after 400 μsec[36]; experimentally there was no measurable heat loss for 25 μsec. Since the growth rates were all measured before 15 μsec none of these end effects was expected to influence them.

The detailed distribution of the mass along the plasma has only a small effect on the growth rate, as found by computing $\omega_{m=1}$ with various axial mass distributions. The assumptions of constant total mass, suggested by $V_{m=1} > V_{m=0}$, rather than constant density, suggested by thermal conduction and flow (see Sec.II) is not a significant source of error. The present experiment contrasts strongly with those in short coils, where axial equilibrium is never reached and flow removes mass from the system.

The theory is for a plasma with a square distribution of $\beta(r)$ rather than the observed Gaussian distribution. The consequent use of an average $\langle\beta\rangle$ in the comparison is not an important source of error since the growth rate is insensitive to beta at the values in the experiment and the errors in the averaging procedure are less than those in the measurement of beta on the axis.

The most important assumption concerns the extent to which the experimentally set up bulged region is in equilibrium, i.e. with no tendency for any lateral motion due to a local "toroidal" curvature and with no pressure gradients or flow along the field lines (i.e. axial equilibrium). The measured vacuum field distribution (Sec.III.B) is expected, for the low value of $\langle\beta\rangle$ in the present experiment,

to give a reliable indication to the field asymmetry with plamsa present, which was not measured. Since the axial average of this asymmetry is negligibly small, the assumption of lateral equilibrium is justified.

The largest difference between the theoretical model and the experiment is due to the continued growth of the bulge as the instability develops. Experimentally we require that the unstable configuration should develop sufficiently slowly to give axial equilibrium but in a time short compared with the instability growth time. However, since the growth time becomes smaller for larger bulges these requirements are incompatible and a compromise was chosen. In all cases δ increased with time due to the bulge growth and this, together with the axial flow, has not been taken into account in the theory. For comparison with theory we have replaced $\delta(t)$ by an effective value δ_{eff} (see Sec.IV).

We shall now examine the comparison between theory and experiment. Firstly, for large bulges (i.e. $B_2/B_1 < 0{\cdot}75$) $\omega_{m=1}$ tends to become independent of δ_{eff} (Fig.7) and to be independent of time (Fig.6) during the growth of the instability, when the bulge itself is still growing (Fig.3). The choice of δ_{eff}, as defined in Sec.IV, while appropriate for small bulges is an underestimate for large bulges (see Fig.3); thus the above-mentioned trend for the growth rate to saturate is even more pronounced than is apparent from Fig.7. Although the condition of Eq.(5) for wall stabilisation is not satisfied, for large bulges beta becomes close to unity[41] and r_p/r_w increases so that the walls should be taken into account. In addition, although no data was included which had been taken after the plasma visibly touched the tube walls, the wings of the diffuse

radial density distribution may have interacted with the wall to give "line shorting" or to modify the external magnetic field shape.

For small bulges ($B_2/B_1 \gtrsim 0{\cdot}75$) the effect of the walls is negligible and equilibrium is reached in about one $m = 1$ growth time; thus a reliable comparison between theory and experiment is possible; this shows that for a collisional plasma the $m = 1$ instability of such bulged theta pinch configurations is in good agreement with ideal MHD theory. In addition, since M&S experiments[33-35] are expected to operate at values of $\delta \sim 0{\cdot}2$, the results given here should be relevant to the instability of such systems.

Finally, we consider the observed absence of modes with $m \geqslant 2$ for all values of δ. The considerations given above that neither end effects nor wall effects should influence the instability apply for $m \geqslant 2$. Since such modes are expected, on ideal MHD theory, to grow at about the same rate as $m = 1$ (see Sec.II), it follows that there is a damping or stabilising mechanism. This is most likely to be the effect of finite ion Larmor radius, since $(a_i/r_2)^2 \approx 10^{-2}$ and $\omega_m/\Omega_i \approx 10^{-3}$ (see Eq.(6)).

VII. CONCLUSION

The observed growth rates of the $m = 1$ instability of an axisymmetric MHD unstable bulged region in the midplane of a long theta pinch have been compared with theoretical predictions. The initial equilibrium was set up experimentally in such a way that it fulfilled most of the assumptions of the theoretical model. In particular, the midplane was found to be free of end effects during the observation of the instability growth, and the collisional plasma ($n = 3 \times 10^{16} cm^{-3}$, $T_e = T_i = 120$ eV) was expected to be well described by MHD theory. The growth rate was calculated for the measured parameters of the

bulged region and was found to agree with the observed growth rate to better than the overall uncertainty of a factor of two. The observed propagation of the $m = 1$ wave due to the instability along the plasma column also agree with theory. It is therefore concluded that the $m = 1$ instability of such bulged configurations agrees with the predictions of ideal MHD theory. Higher modes, with $m \geqslant 2$, expected theoretically to be stabilised by finite Larmor radius effects, were not observed for several ideal MHD growth times.

ACKNOWLEDGEMENTS

The authors wish to express their thanks to C.A. Bunting, G.C.H. Heywood, I.K. Pasco and R. Peacock for their help in carrying out the experiments, J. McCartan for helpful discussions, E.P. Butt for information on instability growth with larger coils, R.S. Pease for drawing their attention to the importance of a diffuse current sheath, and to Mrs J.E. Crow for her assistance with the numerical computations.

TABLE I

PARAMETERS OF THE EXPERIMENT

Circuit Parameters		Electrical Characteristics	
Stored energy	= 0·8 MJ	Peak external field B_e	= 20 ± 1 kG
Bank Voltage	= 34 kV	Initial dB/dt	= 6·5 kG μsec^{-1}
Bank capacity	= 1382 μF	Initial E_θ	= 200 V cm^{-1}
Total Inductance	= 8·9 nH	Ringing half period	= 11·0 μsec
		Crowbar 1/e time	= 160 μsec
		Crowbar ripple	= 20%

Coil Dimensions

Total length (32 sections)	Λ = 771 cm
Length of shaped section	L = 24 cm
Bore of coil	= 11 cm
Bore of tube	= 8·3 cm

Measured Plasma properties on axis at peak field in the uniform column: filling pressure: 20 mtorr D_2

Electron temperature	T_e = 120 ± 15 eV
Sound speed	$C_s = (1{\cdot}4 \pm 0{\cdot}1) \times 10^7$ cm sec^{-1}
Electron density	$n_e = (3 \pm 0{\cdot}5) \times 10^{16}$ cm^{-3}
Beta	$\beta_m = 0{\cdot}7 \pm 0{\cdot}2$
Mean free path	$\lambda \simeq 1$ cm
Electron-ion equipartion time	$t_{eq} \simeq 2$ μsec

Average values (see Appendix II)

Sound Speed	$C_s = 1{\cdot}40 \pm 0{\cdot}15 \times 10^7$ cm sec^{-1}
Beta (Eq.(AII.3))	$\langle\beta\rangle = 0{\cdot}38 \pm 0{\cdot}12$
Mean plasma radius (Eq.(AII.1))	$\langle r_p \rangle = 1{\cdot}0 \pm 0{\cdot}1$ cm

APPENDIX I

Using a model described previously[28] we shall calculate the $m = 1$ motion of a theta-pinch on the assumtpion that (i) the axial (z) motion is negligible and (ii) the distortion of the plasma in the (r,θ) plane is negligible. This means that the displacement is of the form $\underline{\xi} = \underline{\xi}_{r,\theta}(z)$ where $\xi_{r,\theta}$ is the displacement in the (r,θ) plane. Furthermore, since the $m = 1$ instability is a long wavelength instability we can assume $R\frac{d}{dz} \ll 1$ where $R(z)$ is the radius of the square density and pressure distributions assumed in the theoretical model. (This distinguishes the plasma radius, R, in the theoretical model from those defined for the experimental plasma (See Appendix II). R_o refers to the uniform region). This means that the characteristic length for axial variations is much greater than the plasma radius.

The kinetic energy of the plasma is given by

$$T = \tfrac{1}{2}\int \rho \left(\frac{\partial \xi}{\partial t}\right)^2 dv \ ,$$

and using the above assumptions

$$T = \frac{\pi}{2}\int R^2 \rho \left(\frac{\partial \xi}{\partial t}\right)^2 dz \ .$$

The potential energy change as given by[28] is

$$\delta W = \frac{1}{8}\int B^2 \left[\beta R \frac{d^2R}{dz^2}\xi^2 + \left(\frac{d}{dz}(R\xi) - 2\xi\frac{dR}{dz}(1-\beta)\right)^2 + (1-\beta)\left(R\frac{d\xi}{dz} - \xi\frac{dR}{dz}\right)^2\right] dz \qquad \ldots \text{(AI.1)}$$

where B is the external axial magnetic field. $\beta(z) = \frac{8\pi p}{B^2}$ and p is the plasma pressure.

The Lagrangian is given by

$$\mathcal{L} = \int L_{dz} = T - \delta W.$$

From Hamilton's principle we have the equation of motion

$$\frac{\partial L}{\partial \xi} - \frac{\partial}{\partial z}\left(\frac{\partial L}{\partial(\partial\xi/\partial z)}\right) - \frac{\partial}{\partial t}\left(\frac{\partial L}{\partial(\partial\xi/\partial t)}\right) = 0$$

and explicitly this is

$$4(\pi R^2\rho)\,\frac{\partial^2\xi}{\partial t^2} = \frac{\partial}{\partial z}\left((2-\beta)B^2R^2\frac{\partial\xi}{\partial z}\right) + \left(4B^2\left(\frac{dR}{dz}\right)^2(1-\beta^2) - 2B^2R\,\frac{d^2R}{dz^2}\,(1-\beta)\right)\xi \qquad \ldots \text{(AI.2)}$$

To describe the growth of an instability completely it is necessary to specify the initial values of ξ and $\frac{\partial\xi}{\partial t}$ as functions of z. The motion would then be determined as a summation over all the normal modes $\hat{\xi}_n(z)e^{\omega_n t}$ of the system. (For convenience we retain the symbol ξ to describe the spatial factor, (and since only $m = 1$ is considered in this Appendix we drop the subscript $m = 1$ used previously). However, we are not interested in the oscillatory parts of the motion and only need to consider the unstable modes. In fact we shall only consider the fastest growing mode and we shall see that, for small amplitude variation in R at least, this is the only unstable mode.

Consider a pinch whose radius is given by

$$R = R_o \qquad z < -\frac{L}{2}\ ,\ z > \frac{L}{2}$$

$$R = R_o + R_1(z) \qquad -\frac{L}{2} < z < \frac{L}{2}$$

where R_1 is of order δ and $\delta \ll 1$.

In the uniform regions

$$B_o^2\,(2-\beta_o)\,\xi'' - 4\pi\rho_o\,\omega^2\xi = 0$$

where the subscript zero refers to the values of the equilibrium quantities in the uniform region. Thus, for unstable modes

$$\xi(z) = \xi\ (\pm\ L/2)\ \exp\left\{ \mp \left(\frac{4\pi\rho_o}{B_o^2} \cdot \frac{\omega^2}{2-\beta_o}\right)^{\frac{1}{2}} \left(z \mp \frac{L}{2}\right) \right\} . \qquad \ldots \text{(AI.3)}$$

Considering the inner region $-\frac{L}{2} < z < \frac{L}{2}$ and expanding in δ, Eq.(AI.2) becomes in zero order

$$B_o^2\ (2-\beta_o)\ \xi_o'' - 4\pi\rho_o\ \omega^2\xi_o = 0$$

where the subscripts refer to the order in δ.

Now since the cylindrical system, $\delta = 0$, is stable we must expand about the marginal mode $\omega_o = 0$. Thus

$$\xi_o'' = 0$$

and in order to have continuity of ξ'/ξ with the outer solution we must have

$$\xi_o = \text{const.}$$

To next order

$$R_o\ (2-\beta_o)\ \xi_1'' - 2R_1''\ (1-\beta_o)\ \xi_o = 0$$

and

$$\xi_1 = 2\ \frac{1-\beta_o}{2-\beta_o}\ \frac{R_1}{R_o}\ \xi_o .$$

Integration of Eq.(AI.2) between $-\frac{L}{2}$ and $+\frac{L}{2}$ gives

$$\omega^2 \int_{-L/2}^{L/2} 4\mu\ \xi\ dz = \left((2-\beta)\ B^2R^2\ \frac{d\xi}{dz}\right)\Bigg|_{-L/2}^{L/2} + \int \left\{ 4B^2 \left(\frac{dR}{dz}\right)^2\ (1-\beta^2) \right. \qquad \ldots \text{(AI.4)}$$

$$\left. - 2B^2R\ \frac{d^2R}{dz^2}\ (1-\beta) \right\} \xi\ dz$$

where the line mass density $\mu = \pi R^2\rho$

Using Eq.(AI.3) to give the boundary terms and keeping each term in leading order

$$\omega^2\mu_o\, L\xi_o = -B_oR_o\,\omega\left((2-\beta_o)\,\mu_o\right)^{\frac{1}{2}}\xi_o + B_o^2(1-\beta_o^2)\left\langle\left(\frac{dR}{dz}\right)^2\right\rangle L\,\xi_o$$

$$+\tfrac{1}{2}\,B_o^2\,(1-\beta_o)\int\frac{dR}{dz}\left(R_o\,\frac{d\xi_1}{dz} - 3\,\frac{dR}{dz}\,\xi_o\right)dz$$

where the last term in Eq.(AI.4) has been integrated by parts and

$$\left\langle\left(\frac{dR}{dz}\right)^2\right\rangle = \frac{1}{L}\int_{-L/2}^{L/2}\left(\frac{dR}{dz}\right)^2 dz.$$

Substituting for ξ_1 we obtain

$$\omega^2\,\mu_o\,L + \omega\,B_oR_o\,\mu_o^{\frac{1}{2}}\,(2-\beta_o)^{\frac{1}{2}} - B_o^2\left\langle\left(\frac{dR}{dz}\right)^2\right\rangle L\,\frac{\beta_o(1-\beta_o)(3-2\beta_o)}{2(2-\beta_o)} = 0.$$

The ratio of the first term to the second is of order $\omega L/V_A$ where $V_A^2 = B_o^2/4\pi\rho_o$, and since $\frac{\omega L}{V_A} \ll 1$ we can neglect the first term. This means that for small δ the inertial effect of the inner region is negligible compared with the "mass loading" provided by the outer region. Thus finally we have

$$\omega = \frac{V_AL}{R_o^2}\left\langle\left(\frac{dR}{dz}\right)^2\right\rangle\,\frac{\beta_o(1-\beta_o)(3-2\beta_o)}{(2-\beta_o)^{\frac{3}{2}}}\,. \qquad \ldots\ (AI.5)$$

Defining the sound speed $C_s = \left(\frac{\gamma p_o}{\rho_o}\right)^{\frac{1}{2}}$ this equation may be written

$$\omega = \left(\frac{2}{\gamma}\right)^{\frac{1}{2}}\frac{C_sL}{R_o^2}\left\langle\left(\frac{dR}{dz}\right)^2\right\rangle\,\frac{\beta_o^{\frac{1}{2}}(1-\beta_o)(3-2\beta_o)}{(2-\beta_o)^{\frac{3}{2}}} \qquad \ldots\ (AI.6)$$

This result was obtained by an expansion in δ and it is possible that there may be other unstable modes for sufficiently large δ. Considering Eq.(AI.1) we see that the first term is the only

term which can be destabilising. For this term to be comparable with the stabilising terms requires δ to be of order unity. For such large values of δ it is therefore possible that there are further unstable axial modes but since Eq.(AI.2), as applied to each normal mode, is a Sturm-Liouville equation, the growth rates of these modes will be smaller than that of the fundamental mode.

Numerical calculations of the growth rate have been made for the case of the single bulged region defined by

$$R = R_0 \left(1 + \delta \left(1 + \cos \frac{2\pi z}{L}\right)\right) \qquad -\frac{L}{2} < z < \frac{L}{2}$$

In Fig.10 values of the dimensionless growth rate L are plotted against δ for $\beta = 0.4$. It is seen that the analytic result for small δ is accurate to better than 10% for δ less than 0.1, that is for $\frac{\Delta R}{R} < 0.2$ where ΔR is the maximum change in R along z. The computed growth rate for the <u>periodic</u> system

$$R = R_0 \left(1 + \delta \left(1 + \cos \frac{2\pi z}{L}\right)\right)$$

is also plotted. It is seen that it approaches that of the single bulge case for large δ. This is due to the fact that for larger δ the eigenfunction becomes increasingly localised towards the unstable region in z and the form of the region outside this is of less importance.

Fig.11 shows the dependence of the growth rate on β_0 for three values of δ. The theory used would predict a maximum in these curves below $\beta_0 = 0.2$ but the calculation is not valid for $\beta_0 \ll 1$.

APPENDIX II

Evaluation of $\langle\beta\rangle$ and r_p

Average values of beta and radius of the experimental plasma, i.e. $\langle\beta\rangle$ and r_p, are defined as the beta and radius of an equivalent plasma with square density and temperature distribution, having the same line density, temperature, and diamagnetism as the experimental plasma. This definition, gives for equal line density,

$$\frac{r_p^2}{2}\langle\beta\rangle = \int_0^{r_w} \beta(r)\, r\,dr \qquad \ldots \text{(AII.1)}$$

and for equal diamagnetism

$$\frac{r_p^2}{2}\left[1 - \sqrt{1 - \langle\beta\rangle}\right] = \int_0^{r_w} \left(1 - \sqrt{1 - \beta(r)}\right) r\,dr \qquad \ldots \text{(AII.2)}$$

which may be solved for $\langle\beta\rangle$ and r_p.

The experimentally observed plasma has a uniform temperature and Gaussian density and pressure distributions. Substituting $\beta(r) = \beta_m \exp(-r^2/r_o^2)$ into Eqs.(AII.1) and (AII.2) gives a series expansion

$$\langle\beta\rangle = \frac{\beta_m}{2}\left(1 + \frac{1}{12}\beta_m + \frac{7}{192}\beta_m^2 + \ldots\right) \qquad \ldots \text{(AII.3)}$$

In the present experiment it is sufficiently accurate to make the approximation $\langle\beta\rangle \approx \beta_m/2$. In this limit $r_p \approx \sqrt{2}\, r_o$ giving $\beta(\text{at } r_p) \approx 0.14\, \beta_m$. Thus r_p was taken from measured density profiles as the point where $n(r)$ fell to 14% of its maximum value. When values of $\langle\beta\rangle$ are quoted they always refer to the uniform region of the column; the values of r_p in the bulged and uniform regions are denoted by r_2 and r_1 respectively.

REFERENCES

1. L.M. Goldman, H.C. Pollock, J.A. Reynolds and W.F. Westendorp, Phys. Rev. Lett. 9, 361 (1962)
2. W.E. Quinn, E.M. Little, F.L. Ribe and G.A. Sawyer, in Plasma Physics and Controlled Nuclear Fusion Research (International Atomic Energy Agency, Vienna, 1966), Vol.1, p.237.
3. U. Schumacher, R. Wilhelm and H. Zwicker, Bull. Am. Phys.Soc.II 12, 1157 (1967).
4. H.A.B. Bodin, T.S. Green, A.A. Newton, G.B.F. Niblett and J.A. Reynolds, in Plasma Physics and Controlled Nuclear Fusion Research (International Atomic Energy Agency, Vienna, 1966), Vol.1, p.193.
5. C. Andelfinger, G. Decker, E. Fünfer, A. Heiss, M. Keilhacker, J. Sommer and M. Ulrich, in Plasma Physics and Controlled Nuclear Fusion Research (International Atomic Energy Agency, Vienna, 1966), Vol.1, p.248.
6. T.S. Green, D.L. Fisher, A.H. Gabriel, F.J. Morgan and A.A. Newton, Phys. Fluids 10, 1663 (1967).
7. A.A. Newton, Nucl. Fusion 8, 93 (1968).
8. T.S. Green and G.B.F. Niblett, Nucl. Fusion 1, 42 (1961).
9. I.F. Kvartskhava, K.N. Kervalidze, G.G. Zukakishvili and Yu.S. Gvaladze, Nucl. Fusion 3, 285 (1963).
10. H.A.B. Bodin, A.A. Newton, N.J. Peacock, Nucl. Fusion 1, 139 (1961).
11. H.A.B. Bodin, Nucl. Fusion 3, 215, (1963), and A. Eberhagen and H. Glaser, Nucl. Fusion 4, 296 (1964).
12. A.C. Kolb, H.R. Griem, W.H. Lupton, D.T. Phillips, S.A. Ramsden, E.A. McLean, W.R. Faust and M. Swartz, Nucl. Fusion Suppl. 2, 553 (1962).

13. M.G. Haines, Advances in Physics 14, 167 (1965).

14. E.M. Little, W.E. Quinn, F.L. Ribe and G.A. Sawyer, Nucl. Fusion Suppl. 2, 497 (1962).

15 A. Heiss, H. Herold and E. Unsold, Bull. Am. Phys. Soc II 12 1158 (1967).

16. J.W. Mather, Nucl. Fusion 1, 233 (1961).

17. C. Andelfinger, G. Decker, E. Fünfer, H. Hermansdorfer, M. Keilhacker, E. Remy, M. Ulrich, H. Wobig and G.H. Wolf, Institut für Plasmaphysik, Garching, Report IPP 1/55 (1966).

18. A.C. Kolb, W.H. Lupton, R.C. Elton, E.A. McLean, M. Swartz and M.P. Young, in Plasma Physics and Controlled Nuclear Fusion Research (International Atomic Energy Agency, Vienna, 1966), Vol.1, p.261.

19. A. Kaleck, H. Kever, L. Konen, P. Noll, K. Sugita, F. Waelbroeck, H. Witulski, Bull. Am. Phys. Soc. II 12, 1154 (1967).

20. H.A.B. Bodin, T.S. Green, G.B.F. Niblett, N.J. Peacock, J.M.P. Quinn, J.A. Reynolds, Nucl. Fusion Suppl. 2, 521 (1962).

21. W. Lotz, E. Remy, G.H. Wolf, Nucl. Fusion 4, 335 (1964).

22. G.H. Wolf, Institut für Plasmaphysik, Garching, Report IPP 1/63 (1967), Culham Laboratory Translation CTO/458 (1968).

23. M.N. Rosenbluth, N.A. Krall and N. Rostoker, Nucl. Fusion Suppl. 2, 143 (1962).

24. J.B. Taylor, J. Nucl. Energy C 4, 401 (1962).

25. L.D. Pearlstein and N.A. Krall, Phys. Fluids 9, 2231 (1966).

26. S. Chandrasekhar, Hydrodynamic and Hydromagnetic Stability (Oxford University Press, 1961).

27. H. Wobig, Institut für Plasmaphysik, Garching, Report IPP 6/57 (1967).

28. F.A. Haas and J.A. Wesson, Phys. Fluids 9, 2472 (1966).

29. F.A. Haas and J.A. Wesson, Phys. Fluids 10, 2245 (1967).

30. H. Wobig, Institut für Plasmaphysik, Garching, Report IPP 6/53 (1966).

31. P. Merkel and A. Schluter, Institut für Plasmaphysik, Garching Report IPP 6/48 (1966).

32. H. Wobig, Proc. Euratom Symposium on Theoretical Plasma Physics, Varenna, 1, 135 (1966).

33. F. Meyer and H.U. Schmidt, Z. Naturforsch. 13a, 1005 (1958).

34. W. Lotz, E. Remy and G.H. Wolf, Nucl. Fusion 4, 335 (1964).

35. R.L. Morse, W.B. Riesenfeld and J.L. Johnson, Plasma Phys. 10, 543 (1968).

36. A.D. Beach, H.A.B. Bodin, C.A. Bunting, D.J. Dancy, G.C.H. Heywood, M.R. Kenward, J. McCartan, A.A. Newton, I.K. Pasco, R. Peacock and J.L. Watson, Culham Laboratory, CLM-P 198 (1969). To be published in Nuclear Fusion (1969).

37a H.A.B. Bodin and A.A. Newton, Phys. Fluids (to be published in Physics of Fluids (August, 1969).

37b H.A.B. Bodin, J. McCartan, A.A. Newton and G.H. Wolf, In Plasma Physics and Controlled Nuclear Fusion Research (International Atomic Energy Agency, Vienna, 1969), Vol.II, p.533.

38. R.L. Morse, Phys. Fluids 10, 1017 (1967).

39. J.A. Reynolds, E.E. Aldridge, M. Keilhacker and G.B.F. Niblett, Phys. Fluids 8, 529 (1965).

40. R.L. Bingham, L.M. Goldman and R.W. Kilb, In Plasma Physics and Controlled Nuclear Fusion Research (International Atomic Energy Agency, Vienna, 1969), Vol.II, p.667.

41. H.A.B. Bodin, E.P. Butt, J. McCartan and G.H. Wolf. Proc. of Third European Conference on Plasma Physics and Controlled Fusion. Utrecht (1969), p.75.

42. G.C.H. Heywood and H.A.B. Bodin, J. Sci. Instr. 1, 11 (1968).

43. J.A. Wesson, In Plasma Physics and Controlled Nuclear Fusion Research (International Atomic Energy Agency, Vienna 1966), Vol.1, p.223.

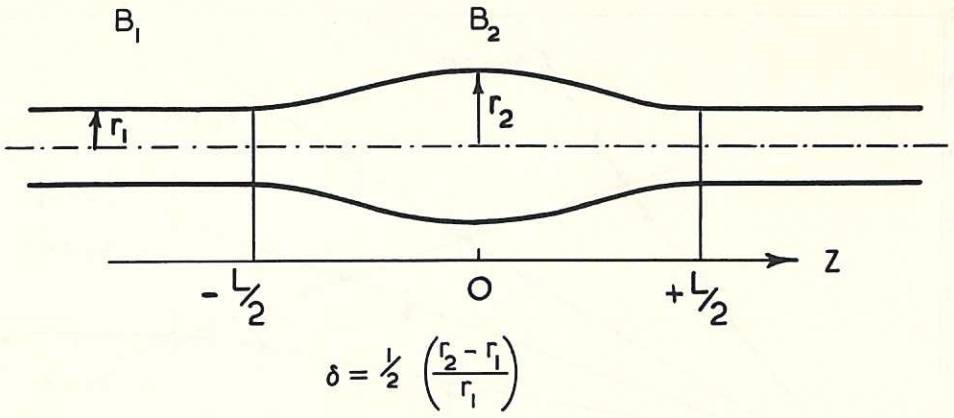

Fig. 1 (CLM-P 184)

MHD unstable equilibrium configuration, where:

$r_p = r_1 \{ 1 + \delta (1 + \cos \frac{2\pi z}{L}) \}$ for $-L/2 < z < +L/2$

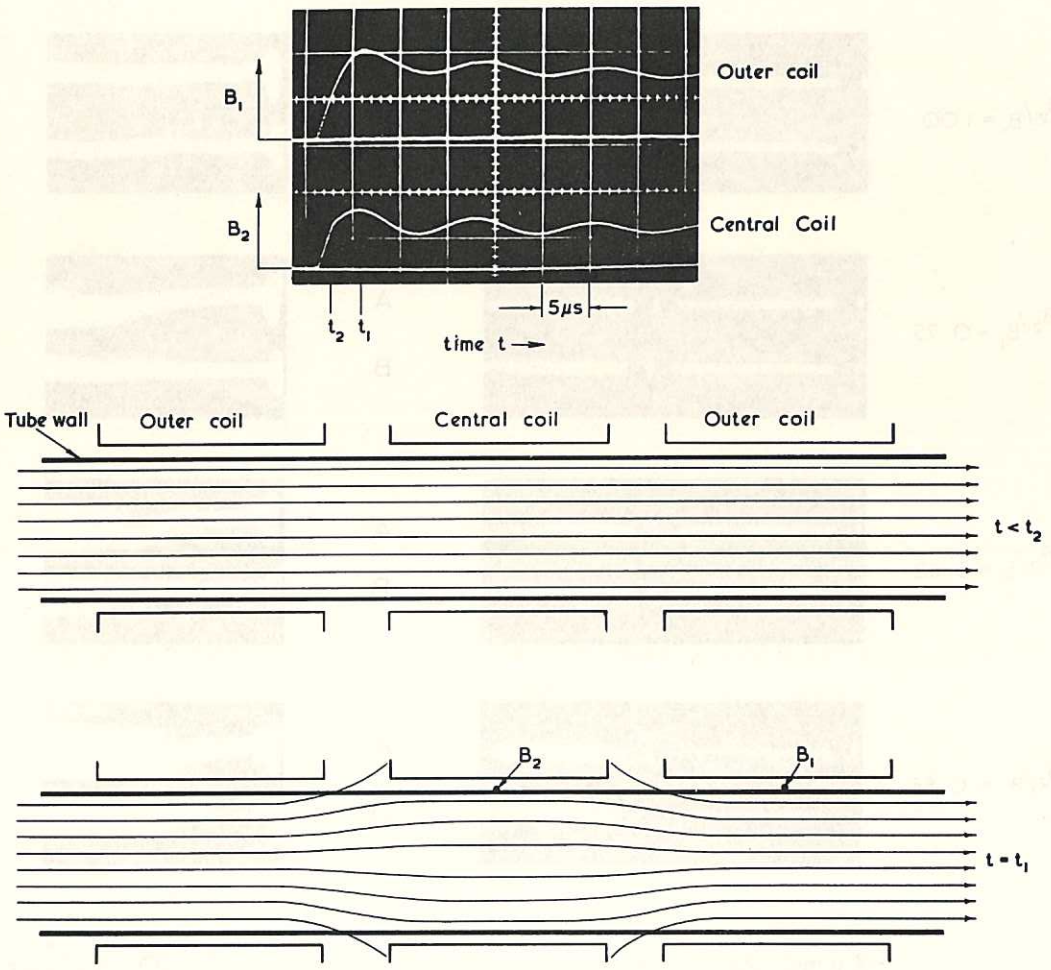

Fig. 2 (CLM-P 184)

Schematic diagram of the method used for generating the unstable bulge, with oscillograms showing the time dependence of the magnetic field

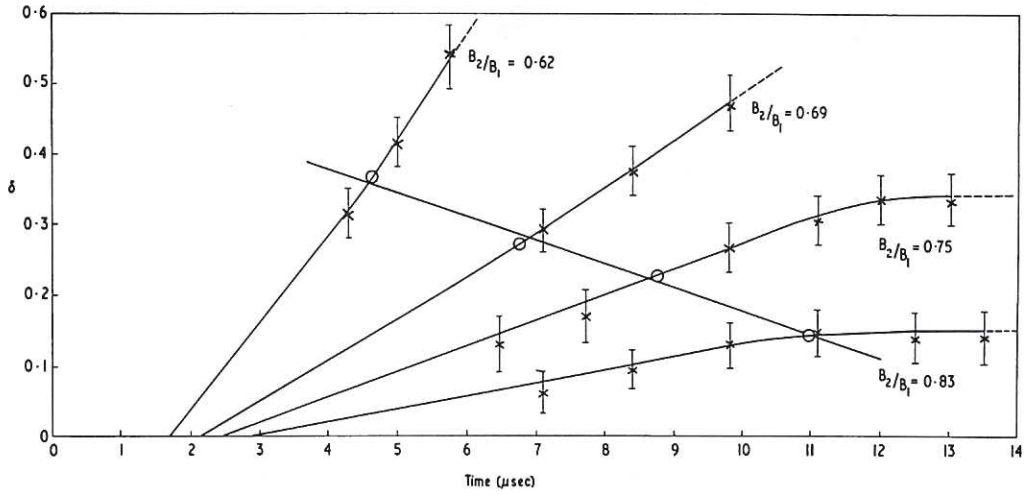

Fig. 3 (CLM-P 184)
Bulge amplitude, δ, as a function of time for various field shaping ratios, B_2/B_1

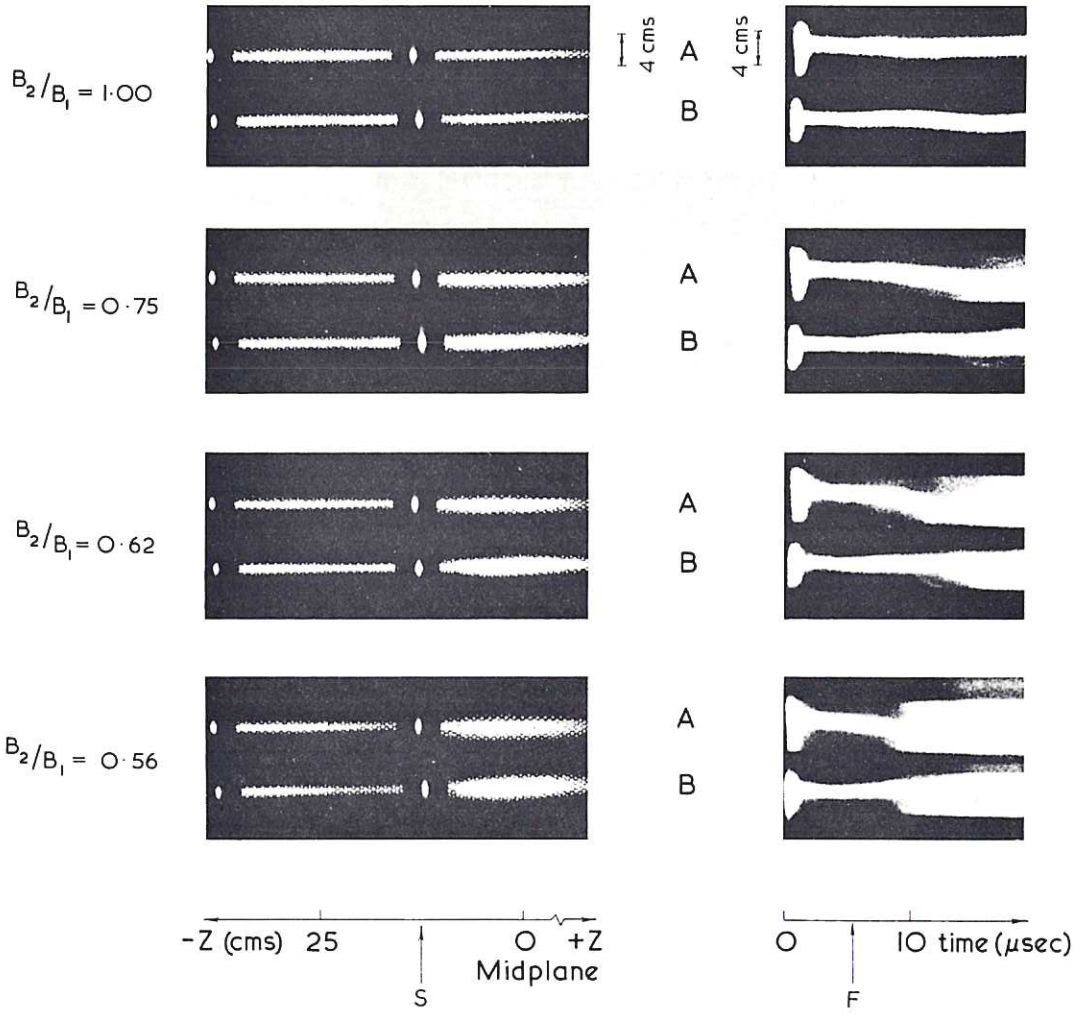

Fig. 4 (CLM-P 184)
Framing (left) and streak (right) camera photographs showing the bulged region and the growth of the m = 1 instability. The top picture shows the case of no unstable bulge, for comparison, and the other three pictures show the plasma behaviour for three different values of the field shaping ratio

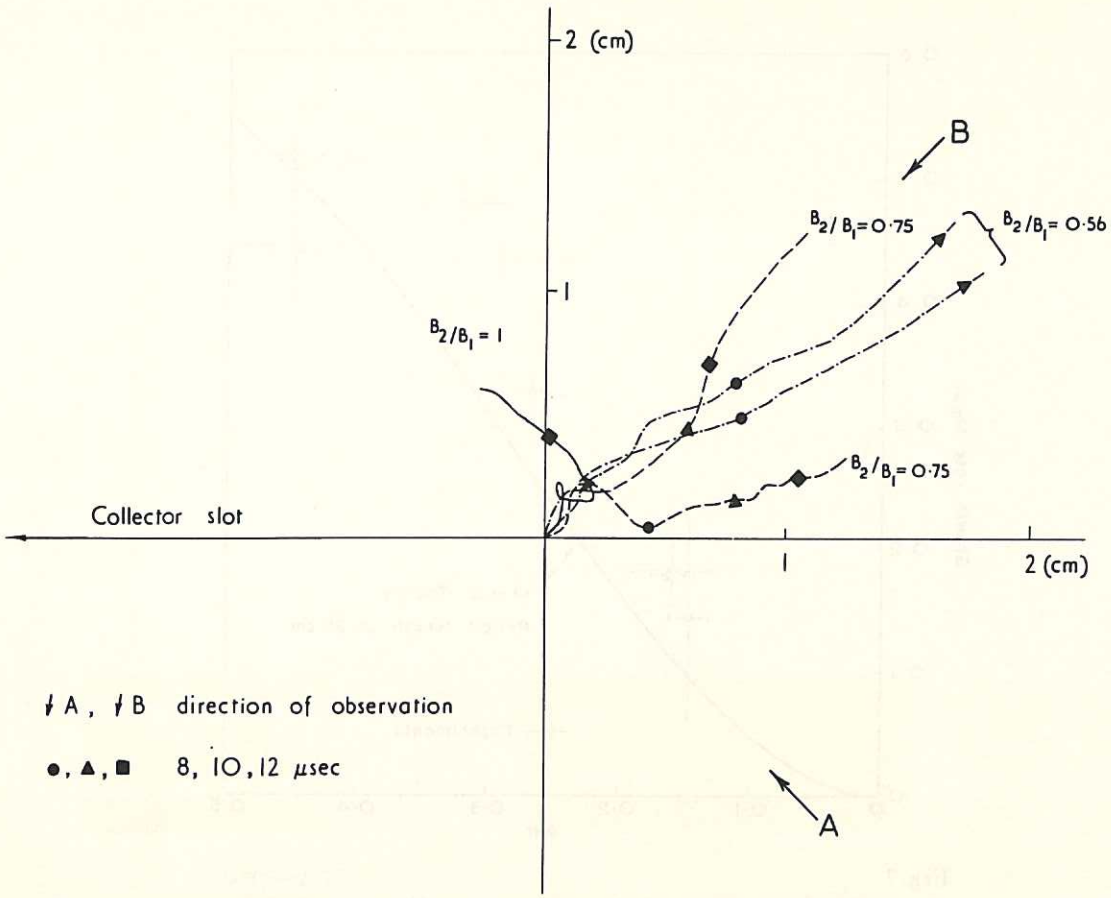

Fig. 5 (CLM-P 184)
The motion of the plasma axis in the r, θ plane during the growth of the instability

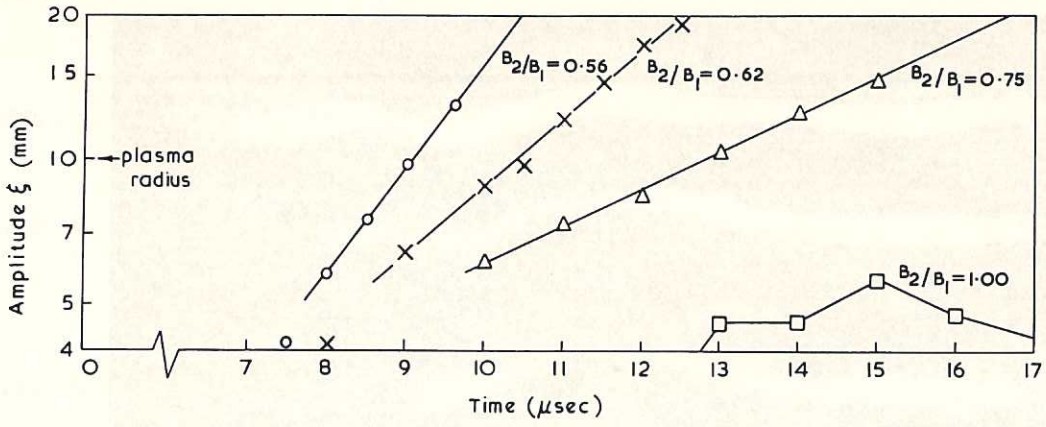

Fig. 6 (CLM-P 184)
The measured amplitude of the $m = 1$ instability as a function of time for different field shaping ratios; ξ is plotted on a long scale

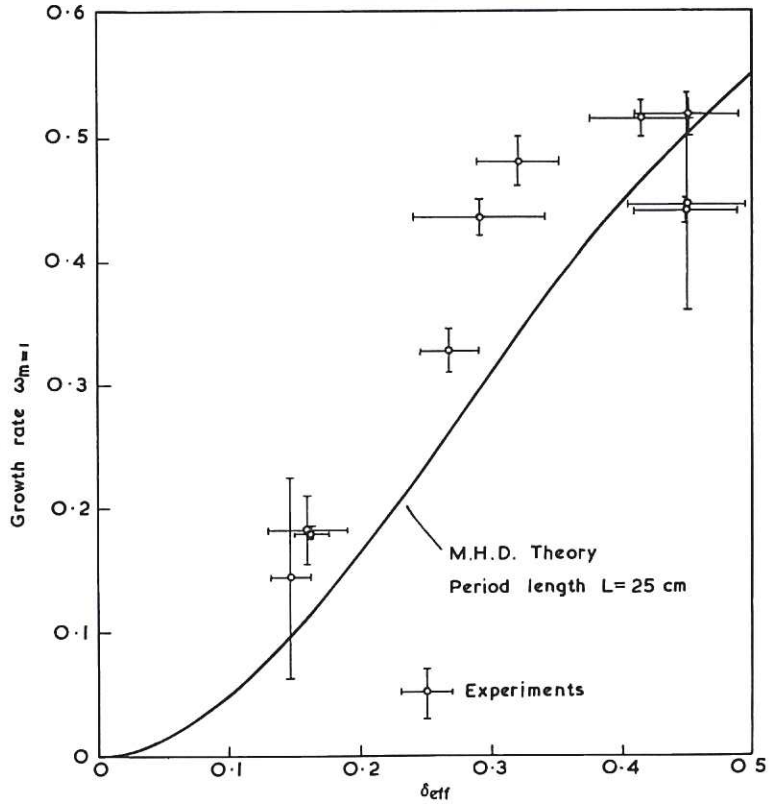

Fig. 7 (CLM-P 184)

The growth rate, $\omega_{m=1}$, of the $m = 1$ instability as a function of the effective bulge strengths, δ_{eff}, showing a comparison between theory and experiment

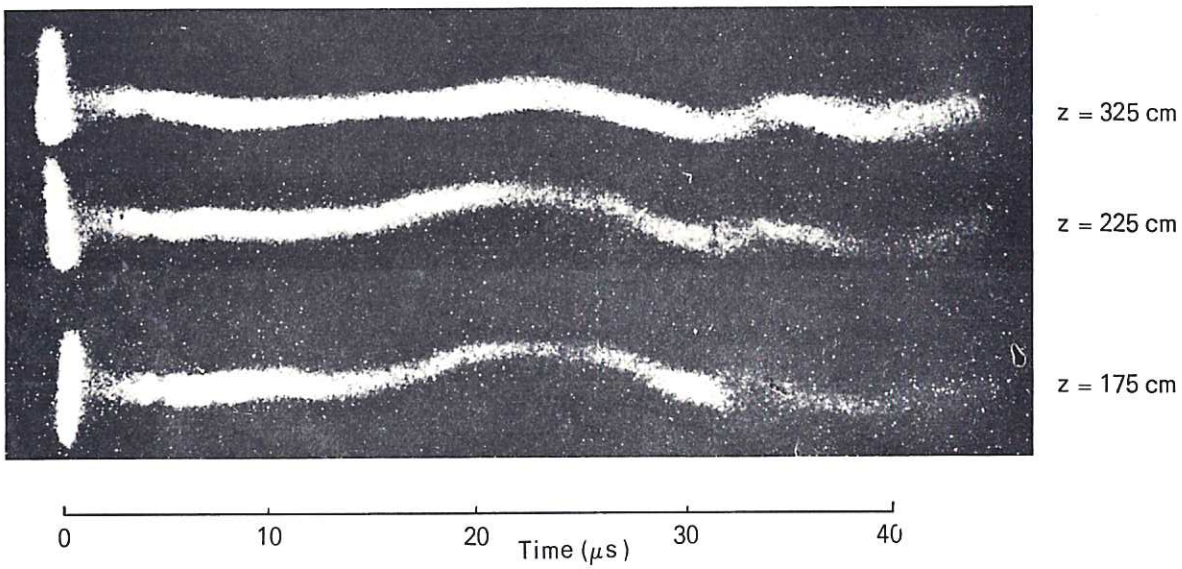

Fig. 8 (CLM-P 184)

Streak photographs at three axial positions showing the propagation of the $m = 1$ wave from the instability axially along the column; z is the distance measured from the midplane of the unstable bulge

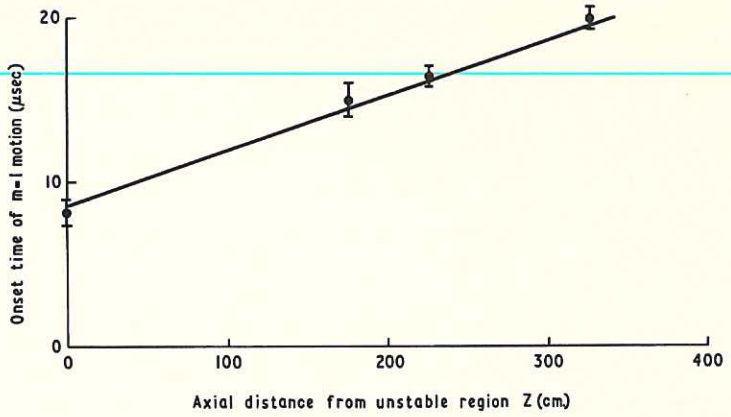

Fig. 9 (CLM-P 184)

Onset time of the m = 1 wave of the instability at different axial positions along the column, measured from the midplane of the bulged region. The line is calculated from measured plasma properties using Eq.3

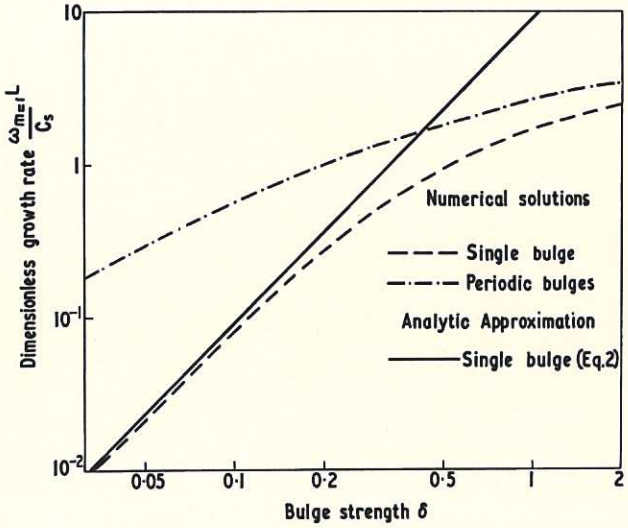

Fig. 10 (CLM-P 184)

Theoretical values of the dimensionless growth rate $\omega_{m=1} L/C_s$ (log scale) as a function of the bulge strength, δ, for $\beta_o = 0.4$. Numerical and analytic solutions for the single bulged region are shown, with, for comparison, the computed variation for the periodic system. (Log scales)

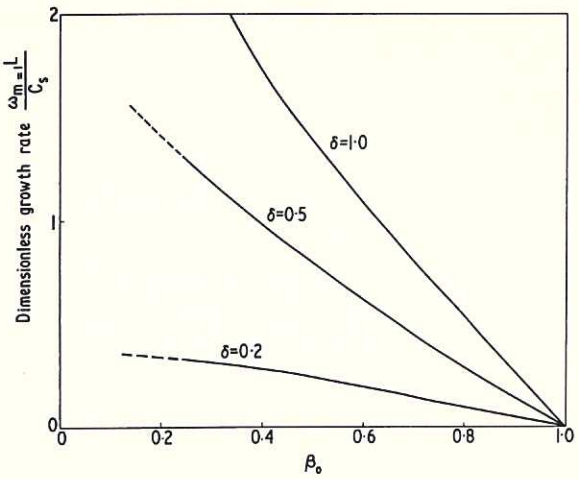

Fig. 11 (CLM-P 184)

Theoretical variation of the dimensionless growth rate $\omega_{m=1} L/C_s$ as a function of β_o for various values of δ for the single bulged configuration